Optical absorption and photoluminescence studies on CdS quantum dots in Nafion

P. Nandakumar and C. Vijayan[a)]
Department of Physics, Indian Institute of Technology, Madras-600036, India

Y. V. G. S. Murti
Department of Physics, Indian Institute of Technology, Guwahati-781001, India

(Received 30 March 2001; accepted for publication 12 October 2001)

Excitonic effects are observed in the optical absorption and photoluminescence of strongly confined CdS quantum dots embedded in the polymer Nafion. The three bands identified in the optical absorption spectra could be attributed to $1s_e$-$1s_h$, $1p_e$-$1p_h$, and $2s_e$-$2s_h$ transitions of the noninteracting particle model. Photoluminescence spectra show a strong emission band corresponding to electron–hole recombination and a weak band due to emission from defect states. The strength of electron–phonon coupling is small in the regime of strong confinement and decreases with decreasing particle size. © *2002 American Institute of Physics.*
[DOI: 10.1063/1.1425077]

I. INTRODUCTION

Physics of quasi-zero-dimensional semiconductor clusters (quantum dots) has attracted considerable interest since the first experimental results of Ekimov and Onuschenko[1] and the theoretical model by Efros and Efros.[2] Quantum size effects associated with the low dimensionality lead to several remarkable modifications in the physical properties of materials.[3–8] These effects are pronounced and lead to a discrete and size-dependent energy level structure when the cluster radius is typically less than the radius of the Bohr orbital of the Mott–Wannier exciton.[2,3] Optical spectroscopic methods play an important role in the study of the quantized energy levels involved.[4–11] There are several aspects of the electronic states in the regime of strong quantum confinement that warrant further scrutiny in spite of the considerable amount of theoretical and experimental results available in this area. In view of this, we have taken up a systematic study of the optical properties of CdS quantum dots in the polymer host Nafion in the regime of strong confinement. The technique of photoacoustic spectroscopy was used to resolve the excitonic transitions in these materials.[12] Studies on the quantum size effects on the optical nonlinearity showed that very large nonlinear susceptibility, predominantly of a nonthermal origin, can be obtained in the strongly confined regime.[7] The present work reports new experimental findings on the quantized energy states of CdS quantum dots as probed by optical absorption and photoluminescence spectroscopy.

II. EXPERIMENTAL DETAILS

CdS quantum dots are synthesized in the polymer matrix Nafion by an ion exchange reaction.[13,14] The detailed preparation procedure is as follows. Nafion 117@ (equivalent weight of 1100) commercially available in the form of films of thickness 0.18 mm cut into suitable sizes are first cleaned in boiling 70% HNO_3 for about half an hour to remove inorganic impurities. This step is followed by repeated washing in boiling water until the pH of the bath is neutral. The films are then soaked in aqueous cadmium acetate solution overnight to facilitate Cd^{2+} ion exchange with protons as confirmed by our electrical transport measurements.[13] The films are then vacuum-dried for about 1 h. Dried films are exposed to ammonia gas for half an hour. This treatment helps in passivating the surface of the quantum dots. The films are dried under vacuum for 1 h and then treated with H_2S gas obtained from a Kipps apparatus for 20 min. The films containing CdS quantum dots are thoroughly dried in vacuum for 1 h.

The size of the quantum dots formed depends on the number of cadmium ions exchanged and hence on the concentration of the cadmium acetate solution. We have varied the concentration of cadmium acetate solution between 0.5 and 0.01 M so as to have quantum dots of sizes 6–1.4 nm.

X-ray powder diffractograms (XRD) of the samples are taken on a Shimadzu horizontal diffractometer. Cu $K\alpha$ radiation was used with the divergence slit, scatter slit, and receiving slit set, respectively, to 1°, 0.1 mm, and 1°. The generator tension was around 40 kV and the current was 30 mA. The diffractograms of the quantum dot samples are recorded in the step-scanning geometry, with a step width of 0.02° and 10 s count time so as to improve the signal-to-noise ratio. XRD of undoped Nafion is taken in the continuous scan mode for the purpose of comparison.

Optical absorption spectra of the samples are recorded on a Hitachi U-3400 recording spectrophotometer in the range 600–200 nm, at a wavelength resolution of 0.1 nm. The spectra are corrected for the base line. Photoluminescence spectra are recorded on a Hitachi F-4500 fluorescence spectrometer. The emission spectra are recorded for different excitation energies greater than the band gap of the samples. Excitation spectra corresponding to the two emission bands

a)Electronic mail: cvijayan@iitm.ac.in

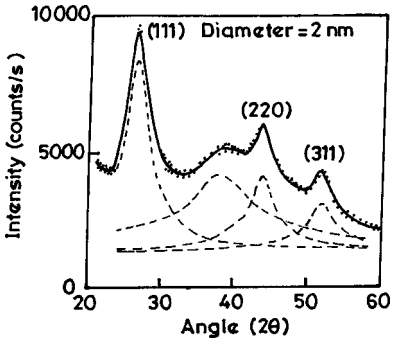

FIG. 1. X-ray diffractrogram (. . .) of CdS quantum dots of diameter 2 nm (sample *S*2) in Nafion along with pseudo-Voigt fit (—). Deconvoluted peaks corresponding to individual reflections are indicated by dashed lines.

observed in photoluminescence emission are also recorded. All the spectra are corrected for the instrumental spectral response.

III. RESULTS AND DISCUSSION

A. X-ray powder diffraction

The XRD of undoped Nafion has an amorphous-like pattern with two wide diffuse maxima located at 15° and 38° (2θ), respectively (Fig. 1). XRD of all the samples reveal diffraction peaks corresponding to the cubic (zinc blende) structural form of CdS, superimposed on the diffuse amorphous background of Nafion. Sample *S*1 contains a small amount of the hexagonal (wurzite) phase of CdS. Compared to the XRD of bulk CdS, the present diffraction lines are generally broad. Among the factors contributing to the broadening are the finite size of the crystallites, strain, and instrumental effects. In order to identify the different contributions to the line broadening and to determine the full width at half maximum (FWHM) of the individual peaks, we have carried out a detailed analysis and decomposition of the XRD profiles using a profile fitting program, PRO-FIT. Figure 1 shows the XRD of sample *S*2 along with the fit and decomposed peaks. The detailed methodology and the results of profile analysis using PRO-FIT are reported elsewhere.[15] The mean diameter of the quantum dots are determined using the Scherrer formula[16]

$$\beta_{\text{size}} = \frac{0.9\lambda}{D\cos\theta}, \tag{1}$$

where λ is the wavelength of the x rays used and β_{size} is the FWHM of the XRD peak corresponding to the Bragg angle 2θ. The analysis shows that the samples studied, denoted as *S*1, *S*2, *S*3, *S*4, and *S*5 contain quantum dots of mean diameters 6, 2, 1.8, 1.6, and 1.4 nm, respectively.

B. Optical absorption

Optical absorption spectra of five samples at room temperature are shown in Fig. 2. Undoped Nafion films do not absorb in the visible range of wavelengths. Bulk CdS crystals are transparent to photon energies below 2.4 eV and the optical absorption spectrum shows a cutoff behavior.[17] The absorption onset is shifted to higher energies as the diameter

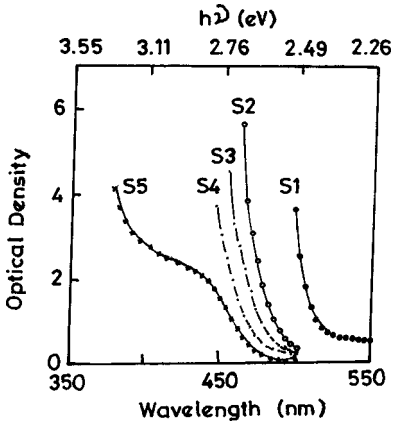

FIG. 2. Optical absorption spectra of CdS quantum dots in Nafion. Mean diameters are 6 nm (*S*1), 2 nm (*S*2), 1.8 nm (*S*3), 1.6 nm (*S*4), and 1.4 nm (*S*5).

of the quantum dot decreases. In samples *S*1, *S*2, *S*3, and *S*4 the absorption increases sharply beyond the absorption edge (taken to be 2.44, 2.54, 2.58, and 2.64 eV, respectively) and no feature could be seen at higher photon energies. The absorption spectrum of sample *S*5 clearly indicates the presence of a broadband located around 2.85 eV. The data on the long wavelength side of this band are fitted to two Gaussian bands by the method of least squares (Fig. 3). Thus the broad shoulder in the absorption spectra in these samples arises out of more than one optical transition. The inset of Fig. 3 shows the spectrum of sample *S*5 recorded at liquid nitrogen temperature (77 K) along with that at room temperature (300 K). On cooling to 77 K the peak (1) in sample *S*5 shifts from 2.88 eV (at room temperature) to 2.94 eV while the peak (2) shifts from 3.09 to 3.18 eV. However, the FWHM of these bands remains practically unchanged. Hence the broadening of the absorption band is not of thermal origin and is probably due to size distribution.

Optical absorption spectra of samples *S*1–*S*4 do not reveal any spectral features beyond the cutoff wavelength. Three-peak structures have been observed in the photoacoustic spectra (PAS) of these samples in our earlier work.[12] The absorption bands were also found to show a blueshift with decreasing quantum dot diameter. The positions of the absorption maxima (A_1,A_2,A_3) and FWHM (Δ_1,Δ_2,Δ_3) of these bands are listed in Table I.

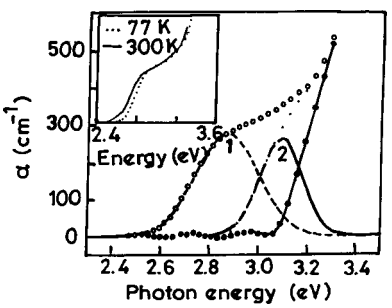

FIG. 3. Optical absorption bands at 300 K in sample *S*5 fitted to two Gaussian bands. The peaks of the two bands are at 2.88 and 3.09 eV. The inset shows the spectra at 77 K along with that at 300 K.

TABLE I. Optical absorption bands of CdS quantum dots.

D (nm)	A_1 (eV)	Δ_1 (eV)	A_2 (eV)	Δ_2 (eV)	A_3 (eV)	Δ_3 (eV)
6	2.54	0.17	2.70	0.29	3	0.64
2	2.66	0.19	2.83	0.35	3.16	0.74
1.8	2.69	0.19	2.86	0.36	3.19	0.74
1.6	2.75	0.22	2.94	0.50	3.34	0.58
1.4	2.77	0.25	3.08	0.63		

The photon energies of the optical transitions obtained from the optical absorption spectra may be compared with those of the bands observed in the photoacoustics spectra. Optical absorption spectra reveal two absorption bands in sample $S5$ located at 2.88 and 3.09 eV. Corresponding to these bands, PAS disclosed bands at 2.77 and 3.08 eV. Considering the large FWHM of the bands, the transition energies obtained from both the methods are in good agreement with each other. The absorption bands in samples $S1-S4$ are inferred from PAS data as the optical absorption spectra reveal no features due to large optical densities. Effective mass approximation (EMA) and tight binding (TB) models[18] lead to transition energies in good agreement with the experimental values in the case of sample $S1$ (diameter 6 nm). However, both the models overestimate the confinement energy for the quantum dots of smaller diameters. Both EMA and TB calculations use parameters relating to the bulk material as numerical inputs and this may be one of the reasons for the discrepancy between the experimental values and theoretical predictions.

C. Noninteracting particle model (NIP model)

Assuming the EMA model to be valid and neglecting the Coulomb interaction, the electron and hole energy levels in quantum dots can be expressed as[2,19]

$$E^h_{n,l} = -\frac{\hbar^2 \xi^2_{n,l}}{2 m_h R^2} \tag{2}$$

and

$$E^e_{n,l} = E_g + \frac{\hbar^2 \xi^2_{n,l}}{2 m_e R^2}, \tag{3}$$

where m_e and m_h denote the effective masses of the hole or the electron, respectively. $\xi_{n,l}$ is the nth zero of the spherical Bessel function. We conveniently express these energy levels in units of eV with the radius R in units of nm as follows:

TABLE II. Optical absorption bands of CdS quantum dots.

D (nm)	A_1 (eV)	Δ_1 (eV)	A_2 (eV)	Δ_2 (eV)	A_3 (eV)	Δ_3 (eV)
6	2.54	0.17	2.70	0.29	3	0.64
2	2.66	0.19	2.83	0.35	3.16	0.74
1.8	2.69	0.19	2.86	0.36	3.19	0.74
1.6	2.75	0.22	2.94	0.50	3.34	0.58
1.4	2.77	0.25	3.08	0.63		

TABLE III. Transition energies.

Energy label	Transition	$\xi_{n,l}$	δE in units of $\frac{h^2}{8\pi^2 R^2 m_r}$
T_1	$1s_e-1s_h$	3.1416	$(3.1416)^2$
T_2	$1p_e-1p_h$	4.4934	$(4.4934)^2$
T_3	$1d_e-1d_h$	5.7635	$(5.7635)^2$
T_4	$2s_e-2s_h$	6.2832	$(6.2832)^2$

$$E^h_{n,l} = -\frac{0.0382}{\mu_h R^2}\xi^2_{n,l} \tag{4}$$

and

$$E^e_{n,l} = E_g + \frac{0.0382}{\mu_e R^2}\xi^2_{n,l}, \tag{5}$$

where μ_h and μ_e represent the effective masses of the hole and the electron, respectively, in units of the electron rest mass. We tabulate the roots $\xi_{n,l}$ and the first few transitions predicted by this noninteracting particle model in Table II.

A quantitative comparison with the experimental results may be made in a way which is independent of the bulk material parameters such as the effective masses and the band gap by adopting the following analysis. We first consider the differences between successive transition energies corresponding to $1s_e$-$1s_h$, $1p_e$-$1p_h$, $1d_e$-$1d_h$, and $2s_e$-$2s_h$ (Table III).

These differences essentially eliminate the bulk band gap E_g. Further we may eliminate the factor containing the effective masses (m_e^* and m_h^*) and the dot radius R by taking the ratios of these differences. The theoretical ratios are then compared with the observed ratios (Table III).

There is good agreement between the theoretical and the observed values of these ratios for all the samples if we assign the first three bands to $1s_e$-$1s_h$ (band A_1), $1p_e$-$1p_h$ (band A_2), and $2s_e$-$2s_h$ (band A_3) transitions. We may note that the observed difference (A_3-A_2) is nearly double the difference (A_2-A_1). The simple noninteracting particle model gives a value of 1.9 for this ratio. On the basis of this assignment we may estimate the values of reduced effective masses (m_r) and the band gap (E_g). These values are given in Table IV.

Since Coulomb interaction and valence band subtleties are ignored in the above picture and the excitons in the nanoparticles are highly confined, such large values for the effective mass are physically acceptable. In the one electron–hole pair picture where the Coulomb attraction between the elec-

TABLE IV. Experimental data.

D (nm)	(A_2-A_1) (eV)	(A_3-A_2) (eV)	$\frac{A_3-A_2}{A_2-A_1}$	$\frac{T_3-T_2}{T_2-T_1}$ (theory)	$\frac{T_4-T_2}{T_2-T_1}$ (theory)
6	0.16	0.30	1.88	1.26	1.87
2	0.17	0.33	1.94	1.26	1.87
1.8	0.17	0.33	1.94	1.26	1.87
1.6	0.19	0.40	2.10	1.26	1.87

TABLE V. Parameters of the NIP model.

D (nm)	m_r/m_0	E_g (eV)
6	0.27	2.39
2	2.32	2.50
1.8	2.87	2.53
1.6	3.24	2.76

TABLE VI. Correspondence between NIP and hybrid models.

Hybrid model	NIP model	Band
$1(S,D)_{3/2}\rightarrow 1s_e$	$1s_h\rightarrow 1s_e$	A_1
$1(P,F)_{3/2}\rightarrow 1p_e$	$1p_h\rightarrow 1p_e$	A_2
$1(D,G)_{3/2}\rightarrow 1d_e$	$1d_h\rightarrow 1d_e$	
$2(S,D)_{3/2}\rightarrow 1s_e$	forbidden	
$2(S,D)_{3/2}\rightarrow 2s_e$	$2s_h\rightarrow 2s_e$	A_3

trons and holes is taken into account, the optical transitions take place between different excited states of the pair. The three absorption bands in the samples should then correspond to transitions from the ground state to the $1s_{(e,h)}$, $1p_{(e,h)}$, and $2s_{(e,h)}$, respectively. However, there will be two major changes if valence band structure is incorporated.[4] The s, p, and d orbitals are no longer pure, but acquire some characteristics of $L+2$ states. Thus the s_h state of the simplified model will be characterized by hybrid hole orbitals (S,D); a p_h state of the simplified model will now become a hybrid (P,F) state since the mixing is between L and $L+2$ states. Second, the forbidden transition for $\Delta n\neq 0$ will acquire a significant oscillator strength because of both the Coulomb potential and the confinement effects. Thus a correspondence may be made between the two models as shown in Table V.

The correspondence between the two models is made by considering the first state (L) to be dominant, i.e., $1(S,D)_{3/2}$ taken to be predominantly of s character, and $1(P,F)_{3/2}$ dominantly p character. The assignment we tentatively suggested earlier in terms of the uncoupled particle model may well be in order if the $1(D,G)_{3/2}\rightarrow 1d_e$ is energetically farther off.

D. Photoluminescence spectra

Figure 4 shows the normalized photoluminescence emission spectra of samples $S1-S5$ corresponding to an excitation at the wavelength 350 nm. The spectra for all samples contain two emission bands. The high energy band (E_1) which is close to the band edge is sharper and more well defined than the second band (E_2) seen at lower energies. The E_1 band exhibits a blueshift with decreasing dot diameter. The long wavelength band (E_2) is weak in intensity and does not show any systematic dependence on the quantum dot size. The peak positions and half widths (Δ_1,Δ_2) found by fitting these bands to Gaussian shape by the method of least squares are given Table VI.

Photoluminescence emission is weak in the case of sample $S1$ (with quantum dots of 6 nm). The two emission bands are very close to each other so that they appear as a single broadband. The excitation spectra of the samples corresponding to the two emission bands (E_1 and E_2) give generally ill-resolved bands (Fig. 5). However, the excitation spectra corresponding to the E_1 band clearly show the presence of multiple bands. These bands show a blueshift with decreasing quantum dot diameter. The first excitation band (closest to the emission band) shifts from 2.5 eV in sample $S1$ to 2.7 eV in sample $S2$ as the diameter of the quantum dots decreases from 6 to 2 nm. The excitation spectra corresponding to the E_2 band also indicate multiple absorption. The first peak in the spectra is located at 2.37 eV and does not exhibit any significant size dependence.

1. Defect emission

Emission bands redshifted from the absorption edge are observed in almost all of the semiconductor clusters studied so far and are generally assigned to defect states.[20,21] These redshifted emissions are usually associated with trapped states such as vacancies, interstitials, impurities, and surface defects. The second lower energy band (E_2) seen in the luminescence spectra of our samples is very weak in intensity when compared to the band edge luminescence. The excitation spectrum corresponding to this emission shows a weak band peaking at about 2.37 eV and clear size dependence is observed. This band is much lower in energy in comparison with the absorption bands of CdS and could be arising from defect levels. The fact that this band does not show any size

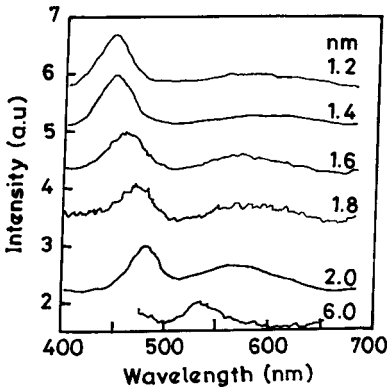

FIG. 4. Normalized PL emission spectra of CdS quantum dots corresponding to 350 nm excitation. The spectra are shifted along the Y axis for clarity.

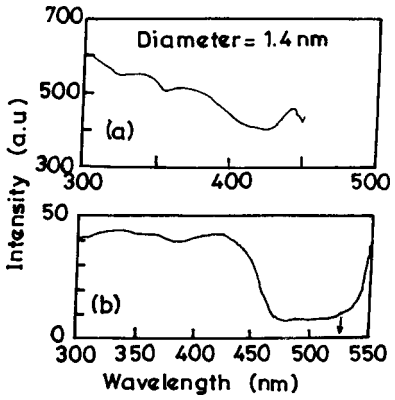

FIG. 5. PL excitation spectra for sample $S5$ corresponding to (a) electron–hole recombination emission and (b) defect emission.

TABLE VII. Photoluminescence bands of CdS quantum dots.

D (nm)	E_1 (eV)	Δ_1 (eV)	E_2 (eV)	Δ_2 (eV)
6	2.32	0.17	2.17	0.11
2	2.59	0.19	2.20	0.32
1.8	2.66	0.28	2.14	0.31
1.6	2.71	0.29	2.17	0.33
1.4	2.77	0.22	2.10	0.31

dependence also indicates that this band cannot be due to exciton absorption. Also, surface passivation by ammonia vapor has resulted in reduced emission intensity of this band indicating involvement of surface defects.

2. Electron–phonon coupling

A comparison of the photon energies of emission and excitation bands relative to the absorption transition energies indicates that the high energy band (E_1) in the emission spectrum has its origin in electron–hole recombination. This is also supported by the fact that the E_1 band shows a blue-shift similar to that observed for the excitonic absorption bands. The peak positions of this band and the observed Stokes shifts (Δ_S) are given in Table VII.

The data given in Table VII show that the Stokes shift (Δ_S) is large (0.22 eV) for the sample $S1$ and smaller for other samples. The relatively large Stokes shift indicates strong coupling to the lattice phonons which may lead to thermal quenching of the luminescence emission. The luminescence observed in sample $S1$ is indeed weak. The Stokes shift for all the other sizes remains small, indicating a weak coupling to lattice phonons in the case of smaller dots. This is again consistent with the relatively large luminescence emission observed for smaller sizes. Following the standard theory of optical absorption and luminescence in the presence of electron–phonon coupling, the Huang–Rhys factor S (or the coupling strength) is given by

$$S=\frac{\Delta_S}{2\hbar\omega_{\mathrm{LO}}}. \tag{6}$$

Theoretical predictions of the size dependence of the electron–phonon coupling are varied; the calculations show constancy, increase, or decrease of the Huang–Rhys factor S with increasing confinement.[22] The Huang–Rhys factor S is deduced for the various dot sizes of our samples in the framework of the configuration-coordinate model, assuming the configuration coordinate corresponds to the longitudinal optical mode of frequency ω_{LO}. Table VII gives the Huang–Rhys factor S for different dot diameters D.

The S factor is the largest for sample $S1$ and the smallest for sample $S5$. We can see that the electron–phonon coupling strength decreases with decreasing particle size in the size range 6–1.4 nm. The estimation of the Huang–Rhys factor on the basis of photoluminescence data may not be quite error-free in view of the fact that the Stokes shift could also have a contribution from relaxation processes into deep trap states. However, the arguments about the size dependence of the coupling strengths could still be qualitatively acceptable. The present findings are in line with those of Shiang *et al.*[23] who reached the same conclusion independently via Raman scattering studies, which are in fact expected to provide better estimates of the coupling strengths. However, the absolute values of S would scale upwards if there are other lower frequency modes ($\omega<\omega_{\mathrm{LO}}$) coupled to the electronic states.

Line broadening in the absorption and emission peaks due to electron–phonon coupling was estimated from the above data. The half-width due to phonon coupling (Δ_P) is related to S by

$$\Delta_P=2\hbar\omega_{\mathrm{LO}}\sqrt{S}. \tag{7}$$

The calculated values of the FWHM (Δ_P) are given in Table VII along with the observed half-width Δ_{expt} and S. These values of half-widths are very small for all samples except for $S1$. This indicates that the line broadening in these samples is mainly due to size effects, in conformity with the analysis of the optical absorption spectra, where we found that the half-widths of the absorption bands are unaffected by cooling to 77 K and are due to the inhomogeneous broadening arising from size dispersion.

IV. SUMMARY

We have synthesized strongly confined CdS quantum dots in the size range 6–1.4 nm and examined their optical properties. The absorption bands are analyzed in terms of the optical transitions predicted by different theoretical models. Quantitative comparison of the observed transition energies with available theoretical calculations indicates good agreement at higher sizes with both EMA and TB models. However, the theoretical estimations deviate considerably from the experimental observations at lower values of dot size. The observed absorption bands are attributed to specific transitions according to the noninteracting particle model. Photoluminescence spectra of the samples contain two bands, one corresponding to direct electron–hole recombination and one attributed to defect-related states. The electron–phonon coupling efficiency is deduced as a function of quantum dot radius by measuring the Stokes shift in the band edge luminescence. Analysis reveals that electron–phonon coupling is weak in quantum dots of smaller sizes. Bands in both optical absorption as well as emission spectra show inhomogeneous broadening owing to the size dispersion of the semiconductor nanoparticles.

ACKNOWLEDGMENTS

The authors thank G. Sundararajan and K. Dhanalakshmi for help in the synthesis of the quantum dot samples. The authors are grateful to Kesavan Nair for interaction on the fitting of the XRD lines through the PRO-FIT software. The financial support from the Inter-University Consortium is acknowledged.

[1] A. I. Ekimov and A. A Onushchenko, Sov. Phys. Semicond. **16**, 775 (1982).
[2] Al. L Efros and A. L. Efros, Sov. Phys. Semicond. **16**, 772 (1982).
[3] Y. Kayanuma, Phys. Rev. B **38**, 9797 (1988).
[4] U. Woggon, *Optical Properties of Semiconductor Quantum Dots* (Springer, Berlin, 1997).

[5] N. Kouklin, S. Bandopadhyay, S. Tereshin, A. Varfolomeev, and D. Zaretsky, Appl. Phys. Lett. **76**, 460 (2000).
[6] I. Mikulskas, E. Bernstein, J. C. Plenet, C. Bovier, R. Tomaiunas, V. Grivickas, T. V. Vaitkus, J. Mugnier, and J. Dummas, Mater. Sci. Eng., B **B69-70**, 418 (2000).
[7] P. Nandakumar, C. Vijayan, and Y. V. G. S. Murti, Opt. Commun. **185**, 457 (2000).
[8] S. M. Oak, K. S. Bindra, R. Chari, and K. C. Rustagi, J. Opt. Soc. Am. B **10**, 613 (1993).
[9] E. P. A. M. Bakkers, E. Reitsma, J. J. Kelly, and D. Vanmaekelbergh, J. Phys. Chem. B **103**, 2781 (1999).
[10] M. Dib, M. Chamarro, V. Voliotis, J. L. Fave, C. Guenaud, P. Roussignol, T. Gacoin, J. P. Boilot, C. Delerue, G. Allan, and M. Lannoo, Phys. Status Solidi B **212**, 293 (1999).
[11] M. Rajalakshmi, A. K. Arora, B. S. Bendre, and S. Mahamuni, J. Appl. Phys. **87**, 2445 (2000).
[12] P. Nandakumar, A. R. Dhobale, Y. Babu, M. D. Sastry, C. Vijayan, Y. V. G. S. Murti, K. Dhanalakshmi, and G. Sundararajan, Solid State Commun. **106**, 193 (1998).
[13] P. Nandakumar, C. Vijayan, Y. V. G. S. Murti, K. Dhanalakshmi, and G. Sundararajan, Indian J. Pure Appl. Phys. **37**, 239 (1999).
[14] P. Nandakumar, C. Vijayan, Y. V. G. S. Murti, K. Dhanalakshmi, and G. Sundararajan, Bull. Mater. Sci. **20**, 579 (1997).
[15] P. Nandakumar, C. Vijayan, Y. V. G. S. Murti, K. Dhanalakshmi, G. Sundararajan, and P. K. Nair, Mater. Sci. Eng., B **B83**, 61 (2001).
[16] B. D. Cullity, *Elements of X-ray Diffraction* (Addison-Wesley, New York, 1977).
[17] M. Cardona, M. Weinstein, and G. A. Wolft, Phys. Rev. A **137**, A1467 (1965).
[18] L. M. Ramaniah and S. V. Nair, Phys. Rev. B **47**, 7132 (1998).
[19] Y. V. G. S. Murti, P. Nandakumar, and C. Vijayan, Phys. Educ. **16**, 229 (1999).
[20] E. F. Hilsinki, P. A. Lucas, and Y. Wang, J. Chem. Phys. **89**, 3435 (1988).
[21] K. Misawa, H. Yao, T. Hayashi, and T. Kobayashi, Chem. Phys. Lett. **183**, 113 (1991).
[22] S. Nomura and T. Kobayashi, Phys. Rev. B **45**, 1305 (1992).
[23] J. J. Shiang, S. A. Risbud, and A. P. Alivisatos, J. Chem. Phys. **98**, 8432 (1993).